

Recension of boron nitride phase diagram based on high-pressure and high-temperature experiments

Ruike Zhang(张瑞柯), Ruiang Guo(郭睿昂), Qian Li(李倩), Shuaiqi Li(李帅琦), Haidong Long(龙海东), and Duanwei He(贺端威)

Citation: Chin. Phys. B, 2024, 33 (**10**): 108103. DOI: 10.1088/1674-1056/ad6a06
Journal homepage: http://cpb.iphy.ac.cn; http://iopscience.iop.org/cpb

What follows is a list of articles you may be interested in

Parameter calculation and result storage for phase-field simulation in α-Mg dendrite growth of Mg-5-wt% Zn alloy

Wei-Peng Chen(陈伟鹏), Hua Hou(侯华), Yun-Tao Zhang(张云涛), Wei Liu(柳伟), and Yu-Hong Zhao(赵宇宏)
Chin. Phys. B, 2023, 32 (**11**): 118103. DOI: 10.1088/1674-1056/acd7e3

High temperature strain glass in Ti-Au and Ti-Pt based shape memory alloys

Shuai Ren(任帅), Chang Liu(刘畅), and Wei-Hua Wang(汪卫华)
Chin. Phys. B, 2021, 30 (**1**): 018101. DOI: 10.1088/1674-1056/abc54a

Superlubricity enabled dry transfer of non-encapsulated graphene

Zhe Ying(应哲), Aolin Deng(邓奥林), Bosai Lyu(吕博赛), Lele Wang(王乐乐), Takashi Taniguchi, Kenji Watanabe, Zhiwen Shi(史志文)
Chin. Phys. B, 2019, 28 (**2**): 028102. DOI: 10.1088/1674-1056/28/2/028102

Phase transition of a diblock copolymer and homopolymer hybrid system induced by different properties of nanorods

Xiao-bo Geng(耿晓波), Jun-xing Pan(潘俊星), Jin-jun Zhang(张进军), Min-na Sun(孙敏娜), Jian-yong Cen(岑建勇)
Chin. Phys. B, 2018, 27 (**5**): 058102. DOI: 10.1088/1674-1056/27/5/058102

Hexagonal boron nitride hollow capsules with collapsed surfaces: Chemical vapor deposition with single-source precursor ammonium fluoroborate

Xiaopeng Li(李肖鹏), Jun Zhang(张军), Chao Yu(郁超), Xiaoxi Liu(刘晓喜), Saleem Abbas, Jie Li(李杰), Yanming Xue(薛彦明), Chengchun Tang(唐成春)
Chin. Phys. B, 2016, 25 (**7**): 078107. DOI: 10.1088/1674-1056/25/7/078107

Recension of boron nitride phase diagram based on high-pressure and high-temperature experiments

Ruike Zhang(张瑞柯)[1], Ruiang Guo(郭睿昂)[1], Qian Li(李倩)[1], Shuaiqi Li(李帅琦)[2], Haidong Long(龙海东)[1], and Duanwei He(贺端威)[1,3,†]

[1] *Institute of Atomic and Molecular Physics, Sichuan University, Chengdu* 610065, *China*

[2] *College of Physics and Electronic Engineering, Chongqing Normal University, Chongqing* 401331, *China*

[3] *Key Laboratory of High Energy Density Physics and Technology of Ministry of Education, Sichuan University, Chengdu* 610065, *China*

(Received 14 February 2024; revised manuscript received 16 July 2024; accepted manuscript online 1 August 2024)

Cubic boron nitride and hexagonal boron nitride are the two predominant crystalline structures of boron nitride. They can interconvert under varying pressure and temperature conditions. However, this transformation requires overcoming significant potential barriers in dynamics, which poses great difficulty in determining the c-BN/h-BN phase boundary. This study used high-pressure *in situ* differential thermal measurements to ascertain the temperature of h-BN/c-BN conversion within the commonly used pressure range (3–6 GPa) for the industrial synthesis of c-BN to constrain the *P*–*T* phase boundary of h-BN/c-BN in the pressure–temperature range as much as possible. Based on the analysis of the experimental data, it is determined that the relationship between pressure and temperature conforms to the following equation: $P = a + \frac{1}{b}T$. Here, P denotes the pressure (GPa) and T is the temperature (K). The coefficients are $a = -3.8 \pm 0.8$ GPa and $b = 229.8 \pm 17.1$ GPa/K. These findings call into question existing high-pressure and high-temperature phase diagrams of boron nitride, which seem to overstate the phase boundary temperature between c-BN and h-BN. The BN phase diagram obtained from this study can provide critical temperature and pressure condition guidance for the industrial synthesis of c-BN, thus optimizing synthesis efficiency and product performance.

Keywords: hexagonal boron nitride, phase diagram, high temperature and high pressure, cubic boron nitride, phase transition, differential thermal analysis

PACS: 81.30.–t, 81.30.Dz, 81.30.Hd, 64.70.–p **DOI:** 10.1088/1674-1056/ad6a06

1. Introduction

Hexagonal boron nitride (h-BN), valued for its outstanding thermal conductivity, chemical stability and electrical insulating properties, is widely used in domains such as electronic devices, lubrication and thermal management.[1–8] The highly regarded cubic boron nitride (c-BN) is known for its extraordinary hardness — second only to diamond — and its impressive thermal and chemical stability.[9–12] These characteristics lead to its wide application as a cutting material for ferrous metals.[13] Much like the transformation from graphite to diamond, h-BN transitions into c-BN under conditions of high pressure and high temperature.[14] The first successful synthesis of c-BN was achieved in 1957 by Wentorf *et al.*, laying the groundwork for constructing the temperature–pressure phase diagram of boron nitride.[15]

The phase diagram, also referred to as a thermodynamic phase equilibrium diagram, concisely outlines the interplay between phase equilibrium composition and factors such as temperature and pressure. The phase diagram of BN, essential for material science and engineering applications, elucidates vital details needed to understand and predict the stable states (such as cubic and hexagonal) of BN under various temperature and pressure conditions. In 1963, Bundy and Wentorf created the initial BN phase diagram based on high-pressure experimental data regarding the h-BN-to-c-BN transformation and melting of h-BN.[16,17] By utilizing computational methods, such as density functional theory and local density or harmonic approximations, Solozhenko *et al.* and Karsten and Kern *et al.* made numerous revisions to the BN diagram.[18–22] Using BN with particle sizes between 0.75 μm and 1.5 μm as a precursor, Eremets *et al.* and the teams of Will and Nover calculated entropy and enthalpy, determining the equilibrium band for c-BN and h-BN phase transitions.[23,24] In 2019, Liang *et al.* employed a flash-heating technique to determine the melting point of c-BN under 15 GPa, which was found to be approximately 5689±411 K.[25,26] In 2021, Zhang *et al.* measured the recrystallization temperature of c-BN, based on its melting point, and inferred from the empirical relationship between recrystallization and melting temperatures that the c-BN melting curve exhibits a slope of about 125 K/GPa in the pressure range 8–16 GPa.[27,28] This indicates potential prior underestimation of the c-BN melting curve temperature.[29] Expanding on the foundational work of Solozhenko *et al.*, in March 2022, Ankudinov *et al.* derived the phase equilibrium line slope for h-BN and c-BN below 4 GPa, resulting in a renewed phase diagram.[30] Upon reviewing the organization of phase diagrams from various historical periods, it becomes evident that these diagrams are constantly

†Corresponding author. E-mail: duanweihe@scu.edu.cn

© 2024 Chinese Physical Society and IOP Publishing Ltd

being revised over time (Fig. 1). In Fig. 1, solid dots represent experimental results, while hollow dots denote computational outcomes. As illustrated in Fig. 1, previous research has primarily focused on utilizing computational simulation methods to determine the phase equilibrium boundaries between c-BN and h-BN. Overall, the BN phase diagram conspicuously lacks support from various experimental data. Furthermore, the figure reveals inconsistencies in the triple-point locations of c-BN, h-BN and their respective liquid states, compounded by fluctuations in the melting curves of c-BN and h-BN. This indicates a general lack of consensus and considerable disorder throughout the entire phase diagram. This study aims to rectify the positions of the phase equilibrium lines between c-BN and h-BN through high-pressure and high-temperature experimental methods, thereby providing a more accurate BN phase diagram with temperature and pressure data. It also serves to supplement the experimental data for the BN phase diagram and organize it more systematically.

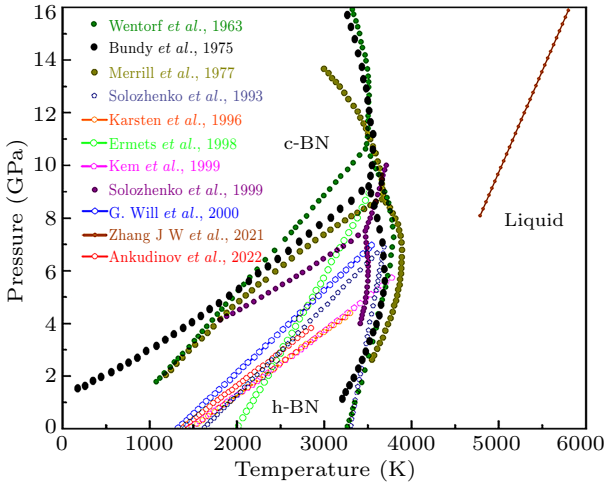


Fig. 1. High-temperature and high-pressure phase diagram of boron nitride. The data come from previous studies.[15–24,31–33] Experimental data are represented using filled symbols, while computed data are represented using open symbols.

Previous studies often employed computational simulation methods to revise the phase equilibrium lines between h-BN and c-BN, and according to our findings, these revisions typically overestimated the temperature of the equilibrium line. Earlier experimental revisions to the BN phase diagram typically used h-BN as a precursor to induce a phase transition to c-BN, delineating the phase equilibrium line based on the phase transition products. This approach is inaccurate. The mutual phase transition between h-BN and c-BN is a diffusion-driven process, involving the disruption and reformation of chemical bonds. Therefore, basing the phase equilibrium line on a single-phase transition line is inaccurate.

This work focuses on high-pressure and high-temperature experiments, employing the high-pressure *in situ* differential thermal analysis (DTA) method to study and constrain the positions of phase equilibrium lines for c-BN and h-BN under high pressure. This method enables a more accurate determination of the phase equilibrium lines of c-BN and h-BN within the high-pressure and high-temperature phase diagram of BN. This study addresses the gaps in the experimental data within the BN phase diagram. Moreover, by integrating the updated data on the melting point of c-BN from Liang and Zhang *et al.*,[26,27] the phase diagram of BN has been refined.

2. Experimental procedures

The chosen pressure points lie between 3–6 GPa, the typical range for industrial c-BN synthesis. The high-pressure and high-temperature (HP-HT) investigations were conducted in a DS6×14 MN cubic press, capable of reaching pressures up to 5 GPa. For experiments beyond 6 GPa, we utilized a two-stage multi-anvil apparatus arranged on the DS6×8 MN cubic press, developed by Sichuan University. The methodology followed was consistent with our previously documented experimental technique. The details of the cell assembly have been included in earlier publications.[34–38]

We applied the *in situ* high-pressure temperature measurement method (HPTM) with differential thermal analysis (DTA) technology, utilizing $W_{97}Re_3$–$W_{75}Re_{25}$ thermocouples manufactured by Shanghai Wolan Instruments, China (with a temperature measurement range of 300 K to 2500 K). The control of temperature is achieved by precisely regulating the power of the electric current, with a control accuracy of 0.01 kW. The setup involved situating one thermocouple at the center of the sample, while assigning the other to an external position as a reference. Since the external temperature remains relatively stable, subtracting the two readings can help highlight the point of sudden temperature change. The formula is

$$\mathrm{DTA} = T_1 - T_2. \tag{1}$$

In this formula, DTA represents the differential thermal value, T_1 is the temperature near the surface of the sample and T_2 is the temperature at the center of the sample. When the sample undergoes an endothermic reaction, the temperature T_2 should decrease, resulting in a noticeable increase in the DTA value. Conversely, when the sample undergoes an exothermic reaction, the temperature should increase, resulting in a noticeable decrease in the DTA value. At the start of a phase transition within the sample, characterized by either heat absorption or release, a significant change in the thermocouple temperature differential was observed.[39] Through soft copper end plugs, the thermocouple was in direct contact with water-cooling tungsten carbide (WC) faces, without using incorporation of cold-junction compensation, as the water-based cooling mechanism cooled the anvils to the target temperature. The heating output was gradually increased in a linear manner over time through an automated process, enabled by a multi-channel data logging apparatus (AX-104, Yokogawa, Japan),

designed specifically for continuous monitoring and recording of temperature changes. The margin of error associated with temperature readings obtained via the thermocouple stood at approximately ±10 K.

The phase equilibrium line is indeed a result of thermodynamics. However, in actual experimental setups, it is unavoidable that kinetic factors will play a role, such as the significant energy barrier between the phase transitions of h-BN and c-BN. This higher energy barrier complicates the direct transformation of h-BN to c-BN in experiments conducted at 3–6 GPa. Consequently, the addition of a catalyst, Li_3N, becomes essential to lower this reaction's energy barrier, facilitating the smooth transition of h-BN into the c-BN phase within its phase region. The catalyst's role is to decrease the energy barrier, effectively reducing the activation energy. The lower the activation energy, the easier the reaction proceeds, enabling the transformation of h-BN into c-BN within the c-BN phase region. To closely approximate the phase transition line effectively, Li_3N powder, sourced from Shanghai Aladdin Bio-Chem Technology Co., LTD, China, with a purity threshold of 99.5%, is employed as the catalyst of choice. Building on initial control experiments and insight from research of Li *et al.*, it is crucial to create an environment approximating hydrostatic conditions within the sample to circumvent the emergence of regions with disparate stress levels that could perturb pressure.[40–42] In the study on the transition of c-BN to h-BN, the sample is enhanced with NaCl to create a hydrostatic environment. A c-BN and NaCl mixture, in a 1:1 mole ratio, using 0–1 μm c-BN particles (obtained from Zhongnan Jiete Ltd., China, purity 99.9%), was used as the precursor for this study.[43] Conversely, for h-BN's transformation into c-BN, a hydrostatic environment essential for the experiment is established through the melting process of the Li_3N catalyst. A blend of 1–2 μm h-BN and Li_3N in a mole ratio of h-BN:Li_3N=1:1 was chosen as the precursor in this experiment (provided by Shanghai Aladdin Bio-Chem Technology Co., LTD, China, with a purity of 99.9%). Finally, to ensure the stability of the phase transition experiment conditions, the heating rate was kept relatively low at 35 K/min.

In this study, the detection of phase transitions between h-BN and c-BN is facilitated using x-ray diffraction, Raman scattering and field emission scanning electron microscopy (FE-SEM; model: JSMIT500HR, JEOL Ltd., Tokyo, Japan). After decompression and cooling, the samples undergo analysis that involves comparing x-ray diffraction peaks and Raman scattering peaks to the standard peak positions of the h-BN and c-BN samples, thereby facilitating phase transformation confirmation. The phase composition data for the recovered samples are obtained by x-ray diffraction (XRD) using Cu-$K\alpha$ radiation (λ = 1.54056 Å, DX-2700) at room temperature. The Raman spectroscopy measurements are carried out with a solid-state laser with a 532 nm wavelength (RGB Laser-systems) and an Andor Shamrock SR-303i-B triple-grating monochromator, equipped with an EMCCD (ANDOR Newton DU970P-BVF).[44]

3. Results and discussion

3.1. Pressure determined via the molten silver method

In the current study, achieving a high degree of precision in pressure control is essential. To this end, the molten silver method is utilized for pressure calibration in the pressure chamber.[45] A silver (Ag) sample is heated in the high-pressure chamber while $W_{97}Re_3$–$W_{75}Re_{25}$ thermocouple monitors keep track of its thermal changes. The appearance of a plateau in the temperature curve indicates the melting of Ag, thereby designating this temperature as the melting point. This observed melting temperature is then compared with existing data on the Ag melting point of Ag variations with pressure, as reported by Akella *et al.*, facilitating the ascertainment of the determination of the real pressure within this particular setup.[46] The black line in the figure illustrates the temperature curve of silver (Fig. 2). The pressure calibration experiment's findings demonstrate a correspondence between varied oil pressures of the press and the resultant pressures of 3.2 GPa, 3.9 GPa, 4.5 GPa, and 5.4 GPa, with a pressure uncertainty of ±0.2 GPa.

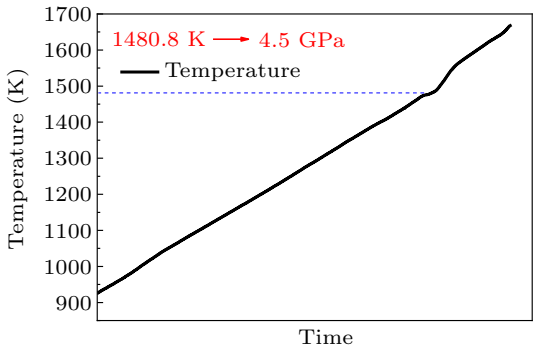


Fig. 2. Example 4.5 GPa: The temperature plateau arises from the melting of silver, from which the actual pressure of this assembly is obtained at 4.5 GPa and 1480.8 K.

3.2. The c-BN transforms into h-BN

A series of heating trials were conducted at varied pressure points, including 3.2 GPa, 3.9 GPa, 4.5 GPa, and 5.4 GPa. Figure 3 shows a gradual increase in the heating power over time, accompanied by a corresponding rise in the c-BN temperature (indicated by the red line). The DTA readings' inflection point (indicated by the black curve) matches the temperature at which the phase transition occurs for c-BN (shown by the red curve). Initial fluctuations in the black line are attributed to NaCl melting within the sample. From a theoretical standpoint, the experiment can be analyzed using the change in Gibbs free energy. The equations for Gibbs free energy and

enthalpy are as follows:

$$G = H - TS, \tag{2}$$

$$H = U + PV. \tag{3}$$

In the formulas, H represents enthalpy, T temperature, S entropy, P pressure and V volume. Considering the changes in Gibbs free energy and enthalpy in this experiment, we can express the formula as follows:

$$\Delta G = \Delta H - T\Delta S = \Delta U - T\Delta S + P\Delta V. \tag{4}$$

In the formula, ΔG represents the change in Gibbs free energy, ΔH represents the change in enthalpy. When ΔG is negative, the phase transition can occur. When the thermodynamic conditions for the phase transition from c-BN to h-BN are met, ΔH will be positive, indicating that the phase transition of c-BN to h-BN under high pressure is an endothermic reaction. The DTA reading (shown as the black line of Fig. 3) is computed by deducting the c-BN sample temperature from the sample's external temperature. This will lead to a rise in the DTA curve.

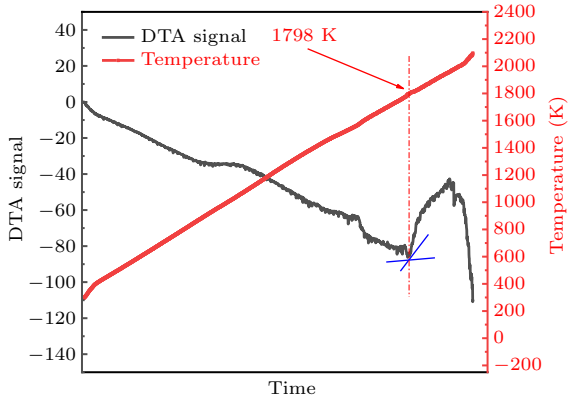


Fig. 3. Example 3.9 GPa: c-BN temperature and DTA reading graph, red line signifies c-BN temperature, black line indicates DTA reading. In transitioning from c-BN to h-BN, the endothermic reaction elevates the DTA curve. At 3.9 GPa, based on the inflection point of DTA, the phase transition temperature of c-BN is 1798 K. Early fluctuations in the black line result from NaCl melting within the sample.

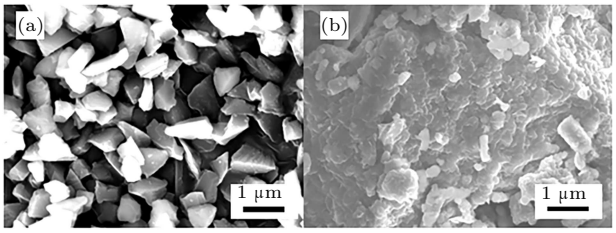


Fig. 4. Example 3.9 GPa: SEM images of c-BN. (a) pre-reaction; (b) post-reaction.

After cooling and decompression, the sample was examined using x-ray diffraction, Raman scattering and SEM, and then compared to standard h-BN. The analysis showed a partial phase transition from c-BN to h-BN (Figs. 4–6). In the XRD diagram, the additional peaks are derived from NaCl. The data indicate that the phase transition of c-BN to h-BN takes place at 1692.7±14 K at 3.2 GPa, 1798±15 K at 3.9 GPa, 1949.9±16 K at 4.5 GPa and 2183.9±19 K at 5.4 GPa.

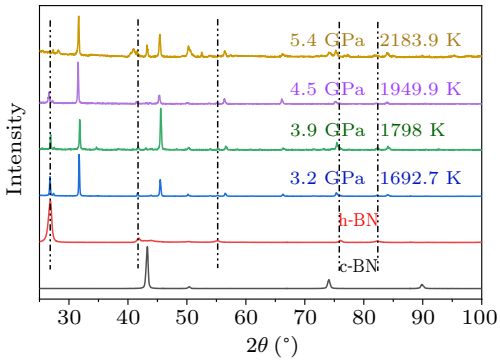


Fig. 5. XRD peaks post-decompression and cooling of initial c-BN and NaCl samples under four pressures. Part of c-BN exhibits a phase transition to h-BN. The other peaks correspond to NaCl.

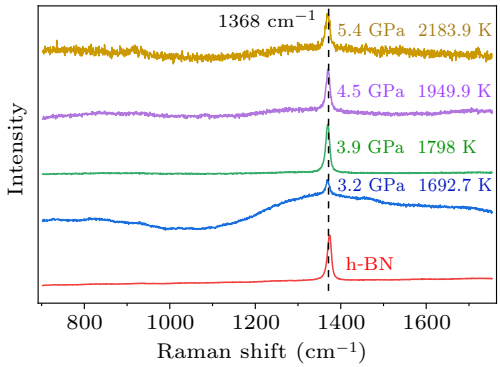


Fig. 6. Raman peaks post-decompression and cooling of initial c-BN and NaCl samples under four pressures. Part of c-BN exhibits a phase transition to h-BN.

3.3. The h-BN transforms into c-BN

Following the approach used in the previous experiment, heating experiments were conducted at the four designated pressure points. Reflecting the analysis presented earlier in this paper, the figure shows both the differential thermal analysis and the h-BN temperature (Fig. 7). Early fluctuations

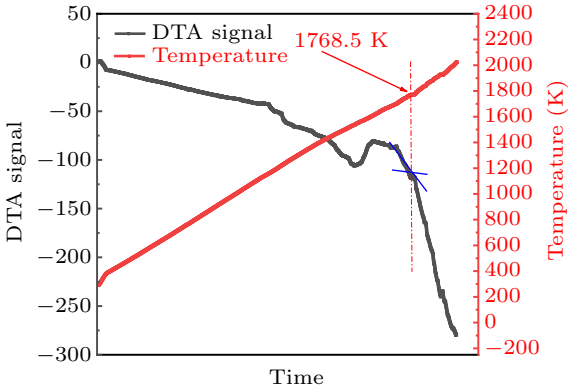


Fig. 7. Example 4.5 GPa: h-BN temperature and DTA reading graph, red line signifies h-BN temperature, black line indicates DTA reading. In the h-BN to c-BN transition, the exothermic process results in a DTA curve decline. At 4.5 GPa, based on the inflection point of DTA, the phase transition temperature of h-BN is 1768.5 K. Initial variations in the DTA curve result from factors such as Li_3N melting.

in the DTA curve stem from factors such as Li_3N melting. According to the equation for the change in Gibbs free energy (Eq. (4)), once the conditions for thermodynamic feasibility of the phase transition from h-BN to c-BN are met, this phase transition is exothermic, causing a decline in the DTA curve. The abrupt changes in temperature, indicated by the black line, align with the phase transition temperatures represented by the red line. The phase transition temperatures for pressures at 3.2 GPa, 3.9 GPa, 4.5 GPa, and 5.4 GPa are 1458.6±11 K, 1559.6±12 K, 1768.5±14 K and 2073.8±18 K, respectively.

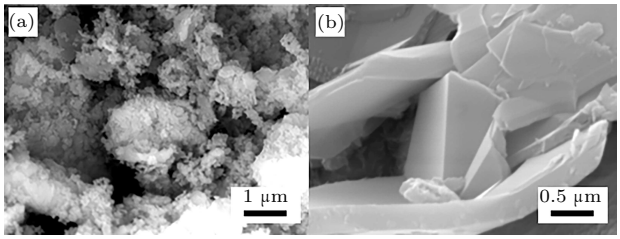


Fig. 8. Example 4.5 GPa: SEM pictures of h-BN. (a) pre-reaction; (b) post-reaction.

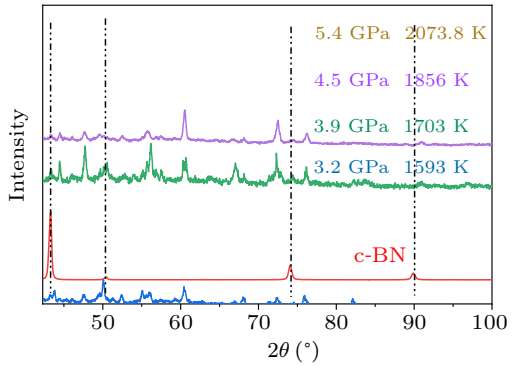


Fig. 9. XRD peaks post-decompression and cooling of initial h-BN and Li_3N samples under four pressures. Part of h-BN exhibits a phase transition to c-BN. Miscellaneous XRD peaks correspond to either Li_3BN_2, a reaction product, or unreacted Li_3N–BN solid solution.

Comparing the temperature data from the phase transition of c-BN to h-BN reveals a comparable temperature range of approximately 240 K at certain pressure points. This significant temperature difference leads to a broader range of the constrained phase equilibrium line, suggesting a discrepancy between the actual phase boundary line and the phase transition line from h-BN to c-BN inferred from the differential thermal analysis. To narrow the range of the constrained phase equilibrium line and achieve the most accurate results, the bisection approach is utilized for the temperature range under identical pressure conditions, thus reducing the enclosed interval. The specimens were then heated to temperatures of 1593 K, 1703 K, 1856 K and 2073.8 K, respectively, at pressure levels of 3.2 GPa, 3.9 GPa, 4.5 GPa and 5.4 GPa, and maintained for 20 min. After decompression and cooling, SEM (Fig. 8), x-ray diffraction (Fig. 9) and Raman scattering (Fig. 10) were employed to examine the sample, which was then compared to standard c-BN. The results indicate a partial phase transition of h-BN to c-BN under each of the four pressure conditions applied. The XRD chart shows various miscellaneous peaks, with some attributed to Li_3BN_2, a byproduct of the reaction, and others recognized as stemming from the unreacted solid solution of Li_3N–BN.

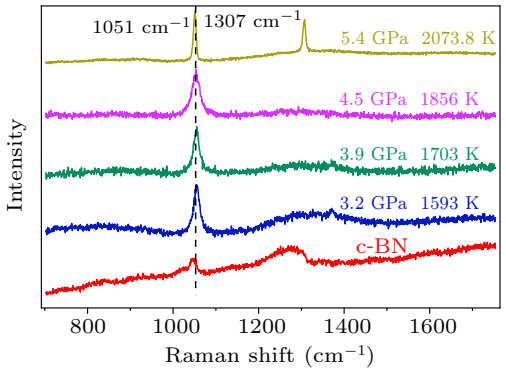


Fig. 10. XRD peaks post-decompression and cooling of initial h-BN and Li_3N samples under four pressures. Part of h-BN exhibits a phase transition to c-BN. Miscellaneous XRD peaks correspond to either Li_3BN_2, a reaction product, or unreacted Li_3N–BN solid solution.

3.4. The revised phase diagram

The phase equilibrium line studied in our experiment is a result of thermodynamics and represents the thermodynamic permission for a phase transition. The mutual phase transition between h-BN and c-BN is a diffusion-driven process, involving the disruption and reformation of chemical bonds. Diffusion-driven phase transitions are the result of atomic rearrangement and, in real experimental processes, are influenced by kinetic factors, such as the energy barrier between h-BN and c-BN. Using the phase transition from h-BN to c-BN as an illustration, it is commonly presumed that BN is in the c-BN phase under experimental conditions within the c-BN phase region. However, due to the presence of a phase transition barrier, h-BN located within the c-BN phase region during the experiment might not convert into c-BN because it fails to overcome the energy barrier. As shown in Fig. 11, for phase transition A, from a thermodynamic standpoint, the energy level before is higher than that after the phase transition. Ideally, if there were no energy barrier, the phase transition would occur seamlessly. However, in reality, phase change only occurs when the energy level prior to the phase change exceeds the energy of the barrier, enabling the formation of the product after the phase change.

Due to the existence of a phase transition barrier, many scientists and technologists are endeavoring to identify more effective catalysts to reduce the barrier, as illustrated in phase transition B in Fig. 11. Within the pressure range of 3–6 GPa, the transformation of h-BN to c-BN is significantly influenced by the presence of a catalyst. The uncatalyzed transformation involves higher bond energies within B–N bonds. Typically, higher temperatures and pressures are necessary to drive the

transformation in the absence of a catalyst. In contrast, catalysts, such as alkali and alkaline earth metal nitrides or fluorides, can effectively lower the phase transition barrier from h-BN to c-BN. They facilitate the breaking of B–N bonds in the h-BN lattice and promote the reorganization of nitrogen and boron atoms, accelerating the nucleation and growth of c-BN. With a catalyst, the transformation can occur at relatively lower temperatures and pressures. However, the use of catalysts can only merely lower, not entirely remove, the phase transition barrier. They lower the required temperature and pressure conditions for the phase transition but do not alter the position of the phase equilibrium line in the phase diagram. Hence, drawing conclusions about the energy levels before and after the phase transition based solely on the post-transition products is not precise. This also contributes to the inaccuracy of the phase regions defined by a single-phase transition pathway (such as h-BN to c-BN or c-BN to h-BN). Due to the energy barrier, previous studies have been unable to derive the phase equilibrium line from a phase transition in a single direction. Our experiment utilizes two phase transition pathways (h-BN to c-BN and c-BN to h-BN) and employs XRD, SEM and Raman spectroscopy to analyze the phase transition products after the experiment. The temperature and pressure conditions of the phase transition were accurately determined using DTA. By establishing two phase transition lines, we outline a "phase equilibrium region". By minimizing this region to be as small as possible, the actual phase equilibrium line between c-BN and h-BN is determined to lie within the phase equilibrium region.

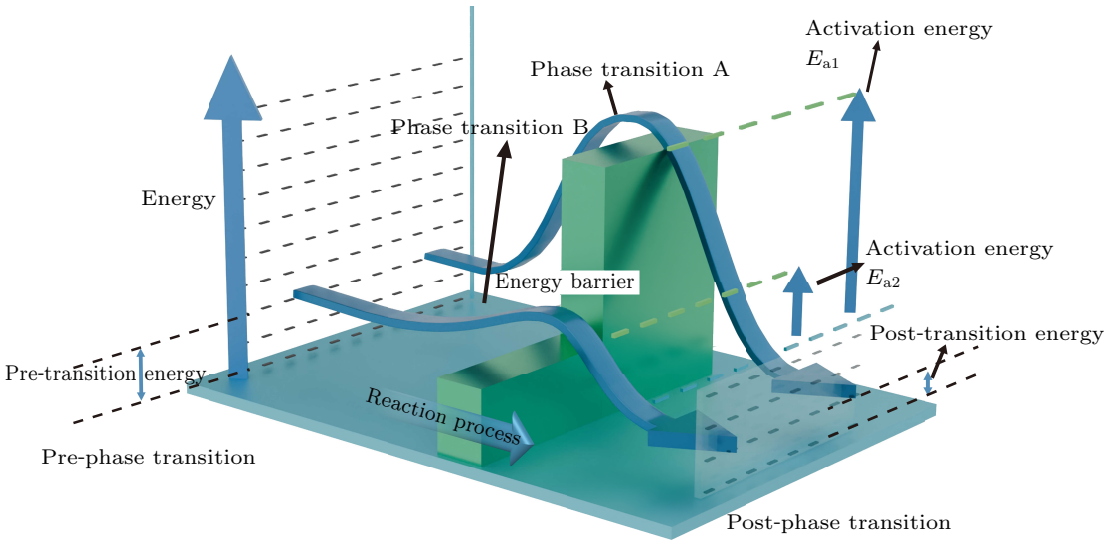


Fig. 11. Phase transition process and potential barrier schematic.[47]

Analyzing and summarizing the content of this study, it is inferred that the phase equilibrium line for c-BN and h-BN at 3.2±0.2 GPa likely lies within the range of 1593±13 K to 1692.7±14 K. When the pressure is increased to 3.9±0.2 GPa, this equilibrium line is anticipated to be between 1703±14 K and 1798±15 K. Proceeding to 4.5±0.2 GPa, it is expected to fall within the 1856±15 K to 1949.9±16 K interval. Finally, at 5.4±0.2 GPa, the phase equilibrium line is projected to reside between temperatures of 2073.8±18 K and 2183.9±19 K (Table 1). Fitted data reveal a linear temperature–pressure correlation for the phase equilibrium of h-BN and c-BN as

$$P = a + \frac{1}{b}T. \tag{5}$$

Here, P denotes pressure (GPa) and T signifies temperature (K). The coefficients are $a = -3.8 \pm 0.8$ GPa and $b = 229.8 \pm 17.1$ GPa/K. The phase boundary line derived from this study is plotted within the phase diagram coordinates. The intercept is denoted as a, indicating that, similar to the graphite/diamond system, h-BN is the stable phase at normal pressure, while c-BN is the metastable phase. According to the Clausius–Clapeyron equation

$$\frac{\mathrm{d}P}{\mathrm{d}T} = \frac{\Delta H}{T\Delta V}. \tag{6}$$

Comparing this with the formula $P = a + \frac{1}{b}T$, we obtain

$$\frac{1}{b} = \frac{\Delta H}{T\Delta V}. \tag{7}$$

Therefore, the constant b can be expressed as

$$b = \frac{T\Delta V}{\Delta H}. \tag{8}$$

Thus, the constant b is related to the temperature, the volume change of the phase transition (ΔV) and the enthalpy change (ΔH). This also implies that the ΔH and the ΔV of the phase transition are independent of temperature. In other words, these thermodynamic parameters remain constant over the entire temperature range.

Table 1. The data points of this experiment.

	h-BN→c-BN	c-BN→h-BN
P (GPa)	T_t (K)	T_t (K)
3.2±0.2	1593±13	1692.7±14
3.9±0.2	1703±14	1798±15
4.5±0.2	1856±15	1949.9±16
5.4±0.2	2073.8±18	2183.9±19

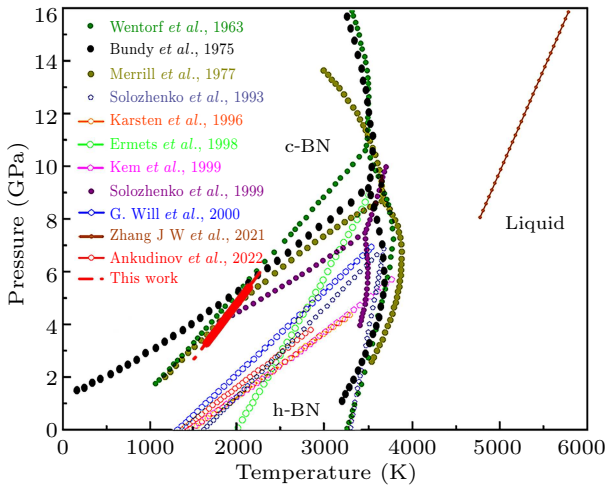


Fig. 12. The HP-HT phase diagram of BN, as amended in this study compared to previous studies. Red solid line, the c-BN/h-BN phase boundary determined and extrapolated from this study. The data come from previous studies.[15–24,31–33] Experimental data are represented using filled symbols, while computed data are represented using open symbols.

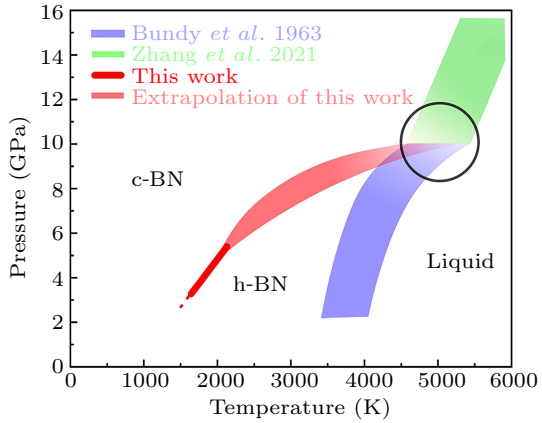


Fig. 13. The phase diagram for boron nitride. Purple area, diagram of Bundy *et al.* in 1963.,[16] and a reasonable extrapolation. Green region, diagram of Zhang *et al.* in 2021.[27] Red solid line and red region, the c-BN/h-BN phase boundary determined and extended by this study.

The phase diagram of BN resulting from this study differs from previous work (Fig. 12). The red solid line represents the area where the experimentally confirmed phase equilibrium line between h-BN and c-BN is found, with an estimated width of 100 K (3–6 GPa). Current high-pressure and high-temperature phase diagrams for BN appear to overestimate the boundary temperatures between c-BN and h-BN phases. Considering the revisions to the c-BN melting curve by Zhang *et al.*, the phase equilibrium line in this research has been appropriately extended (Fig. 12). The green region indicates the findings of Zhang *et al.*[27] The red solid line highlights the contributions of the current study, and the red area depicts the extrapolation of the fitted curve. The purple area showcases the research by Bundy *et al.*, with a logical extrapolation conducted using the data on the melting point of c-BN provided by Zhang *et al.*[16]

4. Conclusion

This study employs *in situ* differential thermal analysis to refine the phase diagram of boron nitride under high-pressure and high-temperature conditions (1000–2300 K and 3—6 GPa), focusing particularly on the phase equilibrium line that separates the c-BN and h-BN phases, crucial for the industrial synthesis of c-BN. As previously discussed, the revised phase equilibrium line essentially forms a "phase equilibrium belt", narrow at just 100 K wide. Given the experimental error margin, this "belt" can be treated as a "line". Our findings bridge the previously identified gaps in experimental data for the high-pressure and high-temperature phase diagrams of BN, providing a sharper picture. The experimental findings suggest that recent computational approaches might overpredict the temperature at the phase equilibrium line. Our data align more closely with the phase diagram derived by Wentorf and Bundy *et al.*, derived from post-reaction product ratio analysis. Notably, our results exhibit greater precision compared to theirs, thus confirming the reliability and accuracy of our experimental methodology. This amendment holds substantial implications for understanding the properties of c-BN and h-BN and their phase transition conduct under high-pressure and high-temperature conditions, and it could profoundly influence the application of c-BN and h-BN in the field of engineering technology.

However, wider phase diagrams reveal challenges, including inconsistencies within the melting curve of c-BN and a scarcity of data on the melting curve of h-BN. Addressing these unresolved issues in subsequent research will enable the scientific community to acquire a more nuanced understanding of BN's phase behavior across various temperature and pressure scenarios. Such advancements will substantially enrich our knowledge and could unveil novel applications for this fascinating material.

Acknowledgement

Project supported by the National Key R&D Program of China (Grant No. 2023YFA1406200).

References

[1] Song Z, Wang W, Cai G and Liu Q H 2018 *Plasmonics* **13** 563
[2] Zhou W, Zuo J, Zhang X and Zhou A 2014 *Journal of Composite Materials* **48** 2517
[3] Perevislov S N 2019 *Refractories and Industrial Ceramics* **60** 291

[4] Kim T Y, Song E H, Kang B H, Kim S J, Lee, Y H and Ju B K 2017 *Nanotechnology* **28** 125207
[5] Turkoglu M, Sahin I and San T 2005 *Pharmaceutical Development and Technology* **10** 381
[6] Decker R, Wang Y, Brar V W, Regan W, Tsai H Z, Wu Q, Gannett W, Zettl A and Crommie M F 2011 *Nano Lett.* **11** 2291
[7] Revabhai P M, Singhal R K, Basu H and Kailasa S K 2023 *Journal of Nanostructure in Chemistry* **13** 1
[8] Shtansky D V, Firestein K L and Golberg D V 2018 *Nanoscale* **10** 17477
[9] Naftaly M, Leist J and Fletcher J R 2013 *Optical Materials Express* **3** 260
[10] Liu T, Kou Z, Lu J, Yan X, Liu F, Li X, Ding W, Liu J, Zhang Q, Wang Q, Ma D, Lei L and He D 2017 *J. Appl. Phys.* **121** 125902
[11] Liu G, Kou Z, Yan X, Lei L, Peng F, Wang Q, Wang K, Wang P, Li L, Li Y, Li W, Wang Y, Bi Y, Leng Y and He D 2015 *Appl. Phys. Lett.* **106** 121901
[12] Yang M, Kou Z L, Liu T, Lu J R, Liu F M, Liu Y J, Qi L, Ding W, Gong H X, Ni X L and He D W 2018 *Chin. Phys. B* **27** 056105
[13] Zhao M, Kou Z, Zhang Y, Peng B, Wang Y, Wang Z, Yin X, Jiang M, Guan S, Zhang J and He D 2021 *Appl. Phys. Lett.* **118** 151901
[14] Mosuang T E and Lowther J E 2002 *Journal of Physics and Chemistry of Solids* **63** 363
[15] Wentorf R H 1957 *The Journal of Chemical Physics* **26** 956
[16] Bundy F P and Wentorf R H 1963 *The Journal of Chemical Physics* **38** 1144
[17] Corrigan F R and Bundy F P 1975 *The Journal of Chemical Physics* **63** 3812
[18] Solozhenko V L 1995 *High Pressure Research* **13** 199
[19] Albe K, Müller W and Heinig K H 1997 *Radiation Effects and Defects in Solids* **141** 85
[20] Solozhenko V L 1993 *Thermochimica Acta* **218** 221
[21] Solozhenko V L 1994 *Diamond and Related Materials* **4** 1
[22] Kern G, Kresse G and Hafner J 1999 *Phys. Rev. B* **59** 8551
[23] Eremets M I, Takemura K, Yusa H, Golberg D, Bando Y, Blank V D, Sato Y and Watanabe K 1998 *Phys. Rev. B* **57** 5655
[24] Will G, Nover G and Von Der Gönna J 2000 *Journal of Solid State Chemistry* **154** 280
[25] Bundy F P and Kasper J S 1967 *The Journal of Chemical Physics* **46** 3437
[26] Liang A, Liu Y, Shi L, Lei L, Zhang F, Hu Q and He D 2019 *Phys. Rev. Res.* **1** 033090
[27] Zhang J, Liu F, Li S, Liang H, Guan S, Wang J, Tian Y, Zhao M and He D 2021 *Journal of the European Ceramic Society* **41** 132
[28] McQueen H J 2004 *Materials Science and Engineering: A* **387–389** 203
[29] De Koker N 2012 *J. Phys.: Condens. Matter* **24** 055401
[30] Ankudinov V and Galenko P K 2022 *Phil. Tran. Roy. Soc. A: Math. Phys. Eng. Sci.* **380** 20200318
[31] Merrill L 1977 *Journal of Physical and Chemical Reference Data* **6** 1205
[32] Solozhenko V L, Turkevich V Z and Holzapfel W B 1999 *The Journal of Physical Chemistry B* **103** 2903
[33] Hu S, Yang J, Liu W, Dong Y, Cao S and Liu J 2011 *Journal of Solid State Chemistry* **184** 1598
[34] Wang J, Tian Y, Su Y, Xiang X, Zhou L, Huang M, Zhang L and He D 2023 *CrystEngComm* **25** 1884
[35] He D W, Zhang F X, Zhang M, Liu R P, Qin Z C, Xu Y F and Wang W K 1997 *Appl. Phys. Lett.* **71** 3811
[36] Liu Y, He D, Wang P, Yan X, Xu C, Liu F, Liu J and Hu Q 2016 *International Journal of Refractory Metals and Hard Materials* **61** 1
[37] Liang A, Liu Y, Liang H, Liu F, Fan C, Zhang J, Wu J, Chen J and He D 2018 *High Pressure Research* **38** 458
[38] Wang J, He D, Li X, Zhang J, Li Q, Wang Z, Su Y, Tian Y, Yang J and Peng B 2020 *Solid State Commun.* **307** 113805
[39] Sachdev, H, Haubner, R, Nöth H and Lux B 1997 *Diamond and Related Materials* **6** 286
[40] He D, He M, Kiminami C S, Zhang F X, Xu Y F, Wang W K and Kuo K H 2001 *J. Mater. Res.* **16** 910
[41] Li Q, Zhang J, Liu J, Tian Y, Liang W, Zheng L, Zhou L and He D 2022 *Diamond and Related Materials* **128** 109241
[42] Guan S, Peng F, Liang H, Fan C, Tan L, Wang Z, Zhang Y, Zhang J, Yu H and He D 2018 *J. Appl. Phys.* **124** 215902
[43] Chen C, Huang R, Wang Z, Shibata N, Taniguchi T and Ikuhara Y 2013 *Diamond and Related Materials* **32** 27
[44] Lei L, Zhang L, Gao S, Hu Q, Fang L, Chen X, Xia Y, Wang X, Ohfuji H, Kojima Y, Redfern S A T, Zeng Z, Chen B, He D and Irifune T 2018 *J. Alloys Compd.* **752** 99
[45] Wang S, He D, Wang W and Lei L 2009 *High Pressure Research* **29** 806
[46] Kennedy G 1971 *Journal of Geophysical Research* **76** 4969
[47] Wang W H 2013 *Progress in Physics* **33** 177